ANALYTICAL BOND MODEL FOR GFRP BARS TO STEEL FIBER REINFORCED SELF-COMPACTING CONCRETE

By H. Mazaheripour,[1] J. A. O. Barros,[2] J. Sena-Cruz,[3] F. Soltanzadeh,[4]

ABSTRACT: The objective of this study is to present a computational algorithm to analytically evaluate the bond behavior between GFRP bar and steel fiber reinforced self-compacting concrete (SFRSCC). The type of information to be derived is appropriate to study the flexural behavior of SFRSCC beams reinforced with GFRP bars in terms of serviceability limit states requirements; in fact the bond between bars and surrounding concrete influences significantly the crack width and crack spacing. The proposed bond model was established by calibrating the parameters of a multi-linear bond-slip constitutive law using the experimental results of pullout bending tests carried out by the authors, taking into account the experimental pullout force *versus* slip at loaded and free ends. According to the comparison between theoretical and experimental pullout force-slip, an acceptable accuracy of the model was observed. Additionally, by considering the proposed bond-slip relationship, a parametric study was carried out to evaluate the influence of the involved bond-slip law's parameters on the maximum force transferred to the surrounding concrete. Finally, the development length of two GFRP bars utilized in the experiments (deformed and smooth bars) was determined by means of the proposed model, and it was compared with the values recommended by codes.

Keywords: GFRP bars, FRC, bond model, pullout bending test

[1] ISISE, PhD student of the Structural Division of the Dep. of Civil Engineering, University of Minho, 4800-058 Guimarães, Portugal. hmp@civil.uminho.pt
[2] ISISE, Full Professor of the Structural Division of the Dep. of Civil Engineering, University of Minho, 4800-058 Guimarães, Portugal. barros@civil.uminho.pt
[3] ISISE, Associate Professor of the Structural Division of the Dep. of Civil Engineering, University of Minho, 4800-058 Guimarães, Portugal. jsena@civil.uminho.pt
[4] ISISE, PhD student of the Structural Division of the Dep. of Civil Engineering, University of Minho, 4800-058 Guimarães, Portugal. f.soltanzadeh@civil.uminho.pt

Introduction

The use of GFRP bars in the construction industry as an alternative reinforcement for concrete structures has increased continuously in the last two decades. Non-conductivity, high strength-to-weight ratio and the superior performance in corrosive environments (e.g. coastline structures) are the most advantages of GFRP bars. However, the relatively low Young's modulus and the lack of yielding phase in stress-strain respond introduce extra challenges in the flexural behavior of concrete members reinforced with GFRP bars, mainly in terms of accomplishing the requirements for serviceability limit states (Gravina and Smith, 2008; Barris et al., 2009). On the other hand, the bond performance of GFRP bars is inferior to steel bars (Choi et al., 2012; Harajli and Abouniaji, 2010). Hence, the serviceability limit states, such as controlling crack width and crack spacing, play a major role in designing GFRP RC structures.

Many attempts have been made to evaluate the bond behavior between GFRP bars and concrete, considering different parameters, e.g. the concrete compressive strength, bar diameter, surface treatment of bar, bar position in cross section of structural element, bond length, temperature change and etc. (Pecce et al., 2001, Tastani et al., 2006, Tang et al., 2008; Baena et al., 2009 and Masoudi et al., 2011). Among these, surface treatment of GFRP bar has been reported as one mostly affects the global bond behavior (He and Tian 2011; Harajli and Abouniaji 2010). Therefore, various surface treatment techniques (e.g. sand-coated, indented, ribbed, helical or wrapping) would provide different interfacial bond behavior. On the other hand, the bond between GFRP bar and concrete is a result of different three bond actions over the interface: chemical cohesion, friction and mechanical interlocking. The chemical bond between GFRP and concrete may be negligible when compared with the other two contributions. In fact, mechanical interlocking (specifically for deformed bar) and friction are dominant bond mechanisms, with an influence level on the bond performance that is dependent on the characteristic of the bar's surface. Theoretically, the bond behavior of GFRP bars is usually presented by a relationship between shear bond stress (τ) and the relative displacement between bar and concrete (i.e. slip). This bond-slip constitutive law is empirically presented by ascending and descending branches, which simulate the bond behavior of the bar before and after peak pullout load, respectively.

The first bond-slip relationship for GFRP bars was presented by Malvar in 1995. Later on, Cosenza et al. (1997) adopted for FRP bars the bond-slip constitutive law proposed by Eligehausen et al. (1983) for steel bars. This model is known as "double branch" and named mBEP (modified Bertero-Eligehausen-Popov). Furthermore, Cosenza et al. (1997) proposed a model with the designation of CMR (Cosenza-Manfredi-Realfonzo) that included a new ascending branch. All these bond-slip constitutive laws, and also other subsequent models (e.g. Zhang et al., 2000; Li et al., 2010) were based on equations that consider the peak bond stress and its corresponding slip derived from pullout force-slip relationships in pullout tests with specific type of bar and surface. Due to the variety of surface characterizations found in available FRP bars, higher difficulties are faced to propose standard constitutive law for the FRP-concrete bond behavior. He and Tian (2011) made an attempt, from the probabilistic standpoint (a database was collected for this purpose), to determine bond

strength of GFRP bars based on reliability analysis. Despite of their efforts to suggest a factor to define the development length of GFRP bars, the analysis does not give idea about the distribution of bond stress and slip throughout the bond length, which is fundamental data for theoretical study on cracking behavior of GFRP RC structures. The database developed by these authors, however, only consider helically wrapped and spirally winded straight GFRP bars, which is very limited since other types of surface such as sand-coated or ribbed GFRP bars are nowadays quite current. Focacci et al. (2000) also defined a rigorous numerical method to calibrate the parameters of a given bond-slip law (they used CMR and mEBP models as example). Firstly, their method still depends on experimental results for calibration; secondly, according to their observations, in the most cases the contact surface between the FRP bar and concrete was highly irregular in consequent of the shape of the bar's surface.

In the light of the above explanation, the correct evaluation of the bond behavior of GFRP bars (FRP in general) still requires experimental verification in order to determine the bond-slip law's parameters for specific bars and surface. This has an extra motivation since GFRP bars are bonded to Steel Fiber Reinforced Self-Compacting Concrete (SFRSCC), forming an innovative composite system.

The present study is part of a research project with the purpose of developing High Performance Steel Fiber Reinforced Self-Compacting Concrete (HPSFRSCC) beams flexurally reinforced by hybrid pre-stressed GFRP and steel bars. GFRP bars are mounted at the bottom tensile surface of the beam while the pre-stressed steel bars are placed with higher concrete cover thickness in order to be protected against corrosive aspects. In this paper, a bond analytical formulation is presented by adopting a multi-linear bond-slip relationship (τ-δ) for two types of GFRP bar's surface (ribbed and sand-coated) embedded in SFRSCC. To calibrate the τ-δ and to appraise the analytical formulation, an extensive experimental program composed of pullout bending test was carried out by the authors. This experimental program was conceived in order to assess the influence of following parameters on the bond behavior: GFRP bar diameter, bar's surface treatment, bond length and SFRSCC cover thickness (Mazaheripour et al., 2012a). Additionally, a parametric study was carried out with the analytical formulation in order to evaluate the influence of involved bond-slip law's parameters on the maximum theoretical force that can be transferred to the surrounding SFRSCC through the bond length. Finally, the minimum theoretical bond length required to achieve the tensile strength of the GFRP bars was determined, and the obtained values are compared with those recommended by some published codes.

Analytical Bond Model

Governing Equation

Neglecting the deformability of surrounding concrete, and assuming a linear and elastic behavior for an embedded bar to concrete, the second-order differential equation that governs the bond behavior along the bond length can be stated as follow (Russo et al., 1990):

$$\frac{d^2\delta(x)}{dx^2} - J_1\tau(\delta(x)) = 0 \tag{1}$$

where J_1 is the ratio between the perimeter (πd_b) and axial stiffness ($E_{lb}\,A_b$) of the bar, being d_b, E_{lb} and A_b the diameter, the longitudinal modulus of elasticity and the cross-sectional area of the bar, respectively. In Eq. (1), $\delta(x)$ represents the slip between GFRP and surrounding concrete at a section x from the free end. Based on the equilibrium condition along the bar, the following equations can also be deduced:

$$\sigma_b(x) = E_{lb}\frac{d\,\delta(x)}{dx} \tag{2}$$

$$\tau(x) = \frac{1}{J_1}\frac{d^2\delta(x)}{dx^2} \tag{3}$$

where σ_b and τ are the axial tensile stress of the bar and the bond shear stress of GFRP-SFRSCC interface respectively.

Local Bond Stress-Slip Relationship

A multi-linear diagram presented in Fig. 1, is proposed as local bond shear stress-slip (τ-δ) relationship for embedded GFRP bar to SFRSCC in this study. This τ-δ relationship is stated by the following equation:

$$\tau(\delta) = \begin{cases} \tau_0 + \dfrac{\tau_m - \tau_0}{\delta_1}\cdot\delta & 0 \le \delta \le \delta_1 \quad (elastic\ phase) \\ \tau_m & \delta_1 < \delta \le \delta_2 \quad (plastic\ phase) \\ \tau_m - \dfrac{\tau_m - \tau_R}{\delta_3 - \delta_2}\cdot(\delta - \delta_2) & \delta_2 < \delta \le \delta_3 \quad (softening\ phase) \\ \tau_R & \delta > \delta_3 \quad (frictional\ phase) \end{cases} \tag{4}$$

The rigid branch (0-τ_0) represents the overall initial shear strength and it is attributable to the micro-mechanical and chemical properties of the involved materials and interfaces. The ascending branch represents the bond behavior between the initial bond shear stress (τ_0) and the bond strength (τ_m) ends at a slip δ_1. Between δ_1 and δ_2, constant bond strength, τ_m, simulates the initiation of the damage in the bar-concrete interface. With the advance of this damage, the bond stress starts decreasing with the increase of slip, and this slip-softening phase, which is governed by friction and micromechanical interlocking along the bond length, is simulated by the third branch that ends at a slip δ_3, when a residual bond shear stress, τ_R, is attained. For $\delta > \delta_3$, due to friction mechanism between bar and surrounding concrete, this residual bond stress is assumed constant, in agreement with previous research (Hao et al., 2008; Baena et al., 2009) and results obtained in the experimental tests.

Theoretical Pullout Force in case of Infinite Bond Length

Debonding process for infinite bond length of GFRP bar is described hereafter by introducing the proposed τ-δ relationship in Eq. (4) into Eq. (1). For each phase, slip distribution along the bar, $\delta(x)$, required bond transfer length,

$L_{tr}(\delta_L)$, and corresponding pullout force at each section of the bar, $F(x)$, are determined for whatever value of loaded end slip (imposed slip, δ_L). These concepts, as well as the definition of the local reference systems in elastic (x^e), plastic (x^p), softening (x^s) and frictional (x^f) bond phases, are illustrated in Fig. 2. The study is based on the works carried out by Bianco et al. (2009) and Sena-Cruz and Barros (2004) in the case of NSM-CFRP laminate.

Elastic phase

When the imposed slip is $\delta_L \leq \delta_1$, Eq. (1) is solved in the local reference system of x^e, and the solution becomes (Bianco et al., 2009):

$$\delta^e(x^e) = C_1^e e^{\lambda x^e} + C_2^e e^{-\lambda x^e} - C_3^e \tag{5}$$

with

$$\frac{1}{\lambda^2} = \frac{\delta_1}{(\tau_m - \tau_0)\cdot J_1} \tag{6}$$

and the particular solution is

$$C_3^e = \frac{\tau_0 J_1}{\lambda^2} \tag{7}$$

By imposing the following boundary conditions into Eq. (5)

$$\begin{cases} \delta^e = 0 \ \text{ at } \ x^e = 0 \\ \delta^e = \delta_L \ \text{ at } \ x^e = L_{tr}^e(\delta_L) \end{cases} \tag{8}$$

where $L_{tr}^e(\delta_L)$ is the bond transfer length corresponding to the first phase ($\delta_L \leq \delta_1$), the integration constants are obtained as follows:

$$C_1^e = \left[\delta_L + C_3^e \cdot \left(1 - e^{-\lambda \cdot L_{tr}^e(\delta_L)}\right)\right] \cdot \frac{1}{e^{\lambda \cdot L_{tr}^e(\delta_L)} - e^{-\lambda \cdot L_{tr}^e(\delta_L)}} \tag{9}$$

$$C_2^e = C_3^e - C_1^e \tag{10}$$

By imposing the equilibrium equation along the bond length (i.e. $F(x = L_{tr}(\delta_L)) = \pi d_b \cdot \int_0^{L_{tr}(\delta_L)} \tau(x^e) dx^e$), $L_{tr}^e(\delta_L)$ becomes:

$$L_{tr}^e(\delta_L) = \frac{1}{\lambda} \cdot \operatorname{arcosh}\left(\frac{\delta_L + C_3^e}{C_3^e}\right) \tag{11}$$

The pullout force at the value of imposed slip can be determined by using Eq. (2)

$$F(x = L_{tr}(\delta_L)) = F^e(x = L^e_{tr}(\delta_L)) = \pi d_b \int_0^{L^e_{tr}(\delta_L)} \tau(x^e) dx^e = E_{lb} A_b \left(\frac{d\delta^e}{dx^e}\right)\Big|_0^{L^e_{tr}(\delta_L)} \quad (12)$$

and the maximum pullout force and maximum bond transfer length undergoing the elastic phase (F_1^e and L_{tr1} respectively) are obtained by imposing a loaded end slip equals δ_1:

$$L_{tr1} = L^e_{tr}(\delta_L = \delta_1) \quad (13)$$

$$F_1^e = F^e(x^e = L_{tr1}) \quad (14)$$

Plastic Phase

The plastic phase corresponds to the loaded end slip in the interval of $\delta_1 < \delta_L \leq \delta_2$ and the corresponding bond shear stress remains constant ($\tau(\delta) = \tau_m$). The solution for Eq. (1) is a polynomial function in the local reference system of x^p as follow

$$\delta^p(x^p) = C_1^p (x^p)^2 + C_2^p x^p + C_3^p \quad (15)$$

with

$$C_1^p = \frac{\tau_m J_1}{2} \quad (16)$$

The boundary conditions are

$$\begin{cases} \delta^p = \delta_1 \text{ at } x^p = 0 \\ \delta^p = \delta_L \text{ at } x^p = L^p_{tr}(\delta_L) \end{cases} \quad (17)$$

where $L^p_{tr}(\delta_L)$ is the bond transfer length in the plastic phase ($\delta_1 < \delta_L \leq \delta_2$) and the integration constants become

$$C_2^p = \frac{(\delta_L - \delta_1) - C_1^p \left(L^p_{tr}(\delta_L)\right)^2}{L^p_{tr}(\delta_L)} \quad (18)$$

$$C_3^p = \delta_1 \quad (19)$$

By imposing the equilibrium equation along the bond length (i.e. $F(x = L_{tr}(\delta_L)) = \pi d_b \cdot \int_0^{L^p_{tr}(\delta_L)} \tau(x^p) dx^p + F_1^e$), $L^p_{tr}(\delta_L)$ is obtained as the following closed-form equation:

$$L^p_{tr}(\delta_L) = \frac{-F_1^e + [F_1^e + 4C_1^p(\delta_L - \delta_1)]^{0.5}}{2C_1^p} \quad (20)$$

and the overall bond transfer length is

$$L_{tr}(\delta_L) = L_{tr1} + L^p_{tr}(\delta_L) \quad (21)$$

The pullout force for whatever value of the imposed slip in this phase is

$$F^{p}(x^{p} = L_{tr}^{p}(\delta_L)) = \pi d_b \cdot \int_0^{L_{tr}^{p}(\delta_L)} \tau_m dx^{p} = \pi d_b \cdot L_{tr}^{p}(\delta_L) \cdot \tau_m \tag{22}$$

and the total pullout force becomes

$$F(x = L_{tr}(\delta_L)) = F_1^{e} + F^{p}(x^{p} = L_{tr}^{p}(\delta_L)) \tag{23}$$

The maximum bond transfer length and maximum pullout force undergoing this phase can be also calculated by substituting δ_L by δ_2 in Eqs. (20) and (22) respectively:

$$L_{tr2} = L_{tr}^{p}(\delta_L = \delta_2) \tag{24}$$

$$F_2^{p} = F^{p}(x^{p} = L_{tr2}) \tag{25}$$

The total force at the end of this phase becomes

$$F_2 = F\left(x = L_{tr}(\delta_L = \delta_2)\right) = F_1^{e} + F_2^{p} \tag{26}$$

Softening Phase

For $\delta_2 < \delta_L \leq \delta_3$, the corresponding bond shear stress, $\tau(\delta_L)$, decreases up to attain the residual bond shear stress, τ_R, at $\delta_L = \delta_3$ (Fig. 1). Introducing into Eq. (1) the corresponding function of Eq. (4) yields a function in the local coordinate system of x^s as follow (Bianco et al., 2009):

$$\delta^{s}\left(x^{s}\right) = C_1^{s} \cdot \sin\left(\beta \cdot x^{s}\right) + C_2^{s} \cdot \cos\left(\beta \cdot x^{s}\right) + C_3^{s} \tag{27}$$

with

$$\frac{1}{\beta^2} = \frac{(\delta_3 - \delta_2)}{(\tau_m - \tau_R)\, J_1} \tag{28}$$

and particular solution becomes

$$C_3^{s} = \frac{\tau_m J_1}{\beta^2} + \delta_2 \tag{29}$$

By considering the relevant boundary conditions of the softening phase

$$\begin{cases} \delta^{s} = \delta_2 & \text{at } x^{s} = 0 \\ \delta^{s} = \delta_L & \text{at } x^{s} = L_{tr}^{s}(\delta_L) \end{cases} \tag{30}$$

where $L_{tr}^{s}(\delta_L)$ is the bond transfer length in the softening phase ($\delta_2 < \delta_L \leq \delta_3$), the integration constants are obtained from

$$C_1^s = \frac{1}{\sin\left(\beta \cdot L_{tr}^s(\delta_L)\right)} \cdot \left\{ \delta_L - \delta_2 + \frac{\tau_m \cdot J_1}{\beta^2} \cdot \left[\cos\left(\beta \cdot L_{tr}^s(\delta_L)\right) - 1 \right] \right\} \tag{31}$$

$$C_2^s = \delta_2 - C_3^s \tag{32}$$

The equilibrium condition along the bond length (i.e. $F(x = L_{tr}(\delta_L)) = \pi d_b \cdot \int_0^{L_{tr}^s(\delta_L)} \tau(x^s) dx^s + F_2^p + F_1^e$) is used to derive the bond transfer length as function of δ_L. So, $L_{tr}^s(\delta_L)$ can be expressed by (Bianco et al., 2009)

$$L_{tr}^s(\delta_L) = \frac{1}{\beta} \cdot \left[\phi + \arcsin \frac{C_s}{\sqrt{(A_s)^2 + (B_s)^2}} \right] \tag{33}$$

with

$$A_s = F_1^e + F_2^p = F_2 \tag{34}$$

$$B_s = \pi d_b \cdot \frac{\tau_m}{\beta} \tag{35}$$

$$C_s = \frac{\pi d_b \cdot \beta}{J_1} \cdot \left(\delta_L - C_3^s \right) \tag{36}$$

and

$$\phi = \operatorname{asin}\left(\frac{B_s}{\sqrt{A_s{}^2 + B_s{}^2}} \right) \tag{37}$$

and the overall bond transfer length at the end of the softening phase is

$$L_{tr}(\delta_L) = L_{tr1} + L_{tr2} + L_{tr}^s(\delta_L) \tag{38}$$

The pullout force for whatever value of imposed slip in this phase is calculated by means of Eq. (39)

$$F^s(x^s = L_{tr}^s(\delta_L)) = \pi d_b \int_0^{L_{tr}^s(\delta_L)} \tau(x^s) dx^s = E_{lb} A_b \left(\frac{d\delta^s}{dx^s} \right) \Bigg|_0^{L_{tr}^s(\delta_L)} \tag{39}$$

and the total pullout force becomes

$$F(x = L_{tr}(\delta_L)) = F_1^e + F_2^p + F^s(x^s = L_{tr}^s(\delta_L)) \tag{40}$$

The maximum bond transfer length and the corresponding pullout force in this phase are calculated for a value of imposed slip equals to δ_3:

$$L_{tr3} = L_{tr}^s(\delta_L = \delta_3) \tag{41}$$

$$F_3^s = F(x^s = L_{tr3}) \tag{42}$$

The total force at the end of the softening phase becomes

$$F_3 = F(x = L_{tr}(\delta_L = \delta_3)) = F_1^e + F_2^p + F_3^s \tag{43}$$

Frictional Phase

When $\delta_L > \delta_3$, $\tau(\delta)$ equals to a constant value of bond shear stress (i.e. τ_R) due to a stable amount of interfacial friction is established between GFRP and surrounding SFRSCC. Therefore, the solution for Eq. (1) is a polynomial function similar to the plastic phase:

$$\delta^f(x^f) = C_1^f (x^f)^2 + C_2^f x^f + C_3^f \tag{44}$$

with

$$C_1^f = \frac{\tau_R J_1}{2} \tag{45}$$

and relevant boundary conditions are

$$\begin{cases} \delta^f = \delta_3 \text{ at } x^f = 0 \\ \delta^f = \delta_L \text{ at } x^f = L_{tr}^f(\delta_L) \end{cases} \tag{46}$$

where $L_{tr}^f(\delta_L)$ is the bond transfer length for $\delta_L > \delta_3$. By imposing these boundary conditions into Eq. (44), the integration constants become

$$C_2^f = \frac{(\delta_L - \delta_3) - C_1^f \left(L_{tr}^f(\delta_L)\right)^2}{L_{tr}^f(\delta_L)} \tag{47}$$

$$C_3^f = \delta_3 \tag{48}$$

and using equilibrium equation (i.e. $F(x = L_{tr}(\delta_L)) = \pi d_b \cdot \int_0^{L_{tr}^f(\delta_L)} \tau(x^f) dx^f + F_3^s + F_2^p + F_1^e$), $L_{tr}^f(\delta_L)$ is calculated by:

$$L_{tr}^f(\delta_L) = \frac{F_3 - [F_3 + 4C_1^f(\delta_L - \delta_3)]^{0.5}}{2C_1^f} \tag{49}$$

The pullout force for whatever value of $\delta_L > \delta_3$ is obtained by using

$$F^f(x^f = L_{tr}^f(\delta_L)) = \pi d_b \int_0^{L_{tr}^f(\delta_L)} \tau_R dx^f = \pi d_b \cdot L_{tr}^f(\delta_L) \cdot \tau_R \tag{50}$$

and the total pullout force is calculated by

$$F(x = L_{tr}(\delta_L)) = F_1^e + F_2^p + F_3^s + F^f(x^f = L_{tr}^f(\delta_L)) \tag{51}$$

Theoretical Pullout Force for Finite Bond Length

In case of finite bond length, the debonding process for embedded GFRP bars (or other types of bars) into concrete can also be analyzed by solving Eq. (1) imposing appropriate boundary conditions for slip at the extremity of the bond transfer length (L_{tr}), which cannot be exceed of an available finite bond length (L_f). While slip at free end (δ_F) is null, i.e. $L_f > L_{tr}$, the pullout force for whatever value of δ_L is directly obtained by using Eqs. (12), (23), (40) and (51). However, when $\delta_F > 0$, i.e. $L_f \leq L_{tr}$, and two or more bond-slip phases are acting over L_f, deriving closed-form equations for pullout force ($F(\delta_L)$) is not straightforward due to the complexity of the equations. To overcome this complexity, Bianco et al. (2009) presented a bond model for NSM-CFRP strips taking a three-linear bond-slip relationship (one ascending and two descending branches) by assuming that the slip distribution ($\delta(x)$) for infinite bond length condition could also be applied to finite bond length condition. That is, the closed-form equations developed for case of infinite bond length were directly used for finite length by considering the possible configurations between L_f and L_{tr} (Bianco et al., 2009). Mazaheripour et al. (2012b) used this bond model by taking a four-linear bond-slip relationship for GFRP bars similar to that which is shown in Fig. 1. Although this model was capable of predicting with good accuracy the pullout force *versus* loaded end slip curves recorded in the experimental tests, the model was not capable to estimate slip at free loaded end, specifically for $L_f > 10d_b$.

In the present study, an analytical-numerical method is presented to determine the pullout force (F) as well as δ_F for whatever value of δ_L in case of a finite bond length (L_f) by taking the relevant boundary conditions at free and loaded ends (i.e. $\delta = \delta_L$ at $x = L_f$ and $\delta = \delta_F$ at $x = 0$) and not assuming the same $\delta(x)$ of infinite bond length condition. Therefore, for each bond phases, new values are derived for those integration constants in Eq. (5), (15), (27) and (44) and, consequently, new $\delta(x)$ is determined over the L_f. The calculation of pullout force, as well as slip at free end for whatever value of imposed slip in case of finite bond length condition is described hereafter by considering different configurations of the proposed bond phases over the L_f.

When One Bond Phase is Acting Over L_f

Fully Elastic

When $\delta_L \leq \delta_1$ and $\delta_1 > \delta_F > 0$, that is, L_f is thoroughly covered by the linear elastic phase (see Fig. 3a); Eqs. (9) and (10) become

$$C_1^e = \left[(\delta_L - \delta_F) + C_3^e \cdot \left(1 - e^{-\lambda \cdot L_f}\right) \right] \cdot \frac{1}{e^{\lambda \cdot L_f} - e^{-\lambda \cdot L_f}} \tag{52}$$

$$C_2^e = (\delta_F + C_3^e) - C_1^e \tag{53}$$

and using equilibrium condition, leads to express δ_F as function of δ_L:

$$\delta_F = \frac{(\delta_L + C_3^e)}{\cosh(\lambda L_f)} - C_3^e \tag{54}$$

The pullout force is calculated by adopting Eqs. (52) and (53)

$$F^e(x^e = L_f) = A_b \sigma_b (x^e = L_f) = E_{lb} A_b \cdot (C_1^e(\delta_L) \cdot \lambda e^{\lambda L_f} - C_2^e(\delta_L) \cdot \lambda e^{\lambda L_f}) \tag{55}$$

Fully Plastic

If $\delta_F > \delta_1$ and $\delta_L \leq \delta_2$, L_f undergoes only the plastic phase (see Fig. 3b). The integration of constants in Eqs. (18) and (19) become

$$C_2^p = \frac{(\delta_L - \delta_F) - C_1^p (L_f)^2}{L_f} \tag{56}$$

$$C_3^p = \delta_F \tag{57}$$

δ_F is also determined by considering equilibrium condition

$$\delta_F = \delta_L - C_1^p (L_f)^2 \tag{58}$$

and F is simply obtained by using

$$F^p(x^p = L_f) = L_f \pi d_b \tau_m \tag{59}$$

Fully Softening

For the case shown in Fig. 3c, L_f fully undergoes softening. Thus, the integration of constants in Eqs. (31) and (32) become

$$C_1^s = \frac{1}{\sin(\beta \cdot L_f)} \cdot \left\{ \delta_L - \delta_F + \frac{\tau_m \cdot J_1}{\beta^2} \cdot [\cos(\beta \cdot L_f) - 1] \right\} \tag{60}$$

$$C_2^s = \delta_F - C_3^s \tag{61}$$

and δ_F can be expressed as function of δ_L by using the equilibrium condition

$$\delta_F = \delta_L - \frac{\tau_m J_1}{\beta^2} \cos(\beta \cdot L_f) + (C_3^s - \delta_2) \tag{62}$$

Therefore, F is obtained by Eq. (62) adopting Eqs. (60) and (61)

$$F^s(x^s = L_f) = \pi d_b \int_0^{L_f} \tau(x^s) dx^s = E_{lb} A_b \left(\frac{d\delta^s}{dx^s}\right)\Big|_0^{L_f} \tag{63}$$

Fully Frictional

If $\delta_F > \delta_3$ and $\delta_L > \delta_3$, the frictional bond phase is acting over L_f (see Fig. 3d). Similar to the fully plastic condition, the integration of the constants in Eqs. (47) and (48) become

$$C_2^f = \frac{(\delta_L - \delta_F) - C_1^f \left(L_f\right)^2}{L_f} \tag{64}$$

$$C_3^f = \delta_F \tag{65}$$

and δ_F is derived as follow

$$\delta_F = \delta_L - C_1^f \left(L_f\right)^2 \tag{66}$$

F is simply obtained by using

$$F^f \left(x^f = L_f\right) = L_f \pi d_b \tau_R \tag{67}$$

When Two or More Bond Phases are Acting Over L_f

When two or more bond phases are acting over the L_f, a numerical strategy was adopted in the present study to obtain the slip and force (or bond stress) distributions. That is, by taking a small increment for the imposed slip at i^{th} step of the calculations (i.e. $\delta_L^i = \delta_L^{i-1} + \Delta\delta_L$) and initially using the value of the pullout force at the last converged step of the calculation, (i-1)th, for each bond phase (i.e. $(F^e)^{i-1}$, $(F^p)^{i-1}$, $(F^s)^{i-1}$ and $(F^f)^{i-1}$), a new value of the pullout force ($F^i = F^{i-1} + \Delta F$) is calculated.

Elastic-Plastic (Fig. 4a)

By imposing δ_L^i, $(L_{tr}^p)^i$ is calculated by Eq. (20) where F_1^e is replaced by $(F^e)^{i-1}$. Being obtained $(L_{tr}^p)^i$, $(L_{tr}^e)^i$ is simply derived by $L_f - (L_{tr}^p)^i$. Therefore, $(\delta_F)^i$ and $(F^e)^i$ are calculated by Eqs. (54) and (55) respectively at $x^e = (L_{tr}^e)^i$. $(F^p)^i$ is also calculated from Eq. (59) at $x^p = (L_{tr}^p)^i$. The total force becomes

$$F^i = (F^e)^i + (F^p)^i \tag{68}$$

Plastic-Softening (Fig. 4b)

For δ_L^i, $(L_{tr}^s)^i$ is calculated by means of Eq. (33) where F_1^e is null and F_2^p is substituted by $(F^p)^{i-1}$. Being obtained $(L_{tr}^s)^i$, $(L_{tr}^p)^i$ is simply obtained by $L_f - (L_{tr}^s)^i$. Therefore, $(F^p)^i$ and $(\delta_F)^i$ are calculated by Eqs. (58) and (59) respectively at $x^p = (L_{tr}^p)^i$. $(F^s)^i$ is also calculated from Eq. (63) at $x^s = (L_{tr}^s)^i$. The total force becomes

$$F^i = (F^p)^i + (F^s)^i \tag{69}$$

Softening-Frictional (Fig. 4c)

Here by imposing an increment for the imposed slip, $(L_{tr}^f)^i$ is calculated by Eq. (49) where F_1^e and F_1^p are null and F_3^s is substituted by $(F^s)^{i-1}$. Being obtained $(L_{tr}^f)^i$, $(L_{tr}^s)^i$ is simply calculated by $L_f - (L_{tr}^f)^i$. Hence, $(F^s)^i$ and $(\delta_F)^i$

are determined by Eqs. (62) and (63) respectively at $x^s = (L_{tr}^s)^i$. $(F^f)^i$ is also determined by Eq. (67) at $x^f = (L_{tr}^f)^i$. The total force becomes

$$F^i = (F^s)^i + (F^f)^i \tag{70}$$

Elastic-Plastic-Softening (Fig. 5a)

For small increment of imposed slip, $(L_{tr}^s)^i$ is calculated by Eq. (33) where F_1^e and F_2^p are substituted by $(F^e)^{i-1}$ and $(F^p)^{i-1}$ respectively. Additionally, $(L_{tr}^p)^i$ is determined by Eq. (20) where F_1^e is also replaced by $(F^e)^{i-1}$.

Therefore, $(L_{tr}^s)^i$ is given by

$$(L_{tr}^e)^i = L_f - (L_{tr}^p)^i - (L_{tr}^s)^i \tag{71}$$

Since free loaded end undergoes elastic bond phase, $(\delta_F)^i$ is calculated by Eq. (54) at $x^e = (L_{tr}^e)^i$. Then, $(F^e)^i$ is calculated by Eq. (55) at $x^e = (L_{tr}^e)^i$, $(F^p)^i$ by Eq. (59) at $x^p = (L_{tr}^p)^i$, and $(F^s)^i$ by Eq. (63) at $x^s = (L_{tr}^s)^i$. The total pullout force becomes

$$F^i = (F^e)^i + (F^p)^i + (F^s)^i \tag{72}$$

Plastic-Softening-Frictional (Fig. 5b)

Similar to the previous configuration, $(L_{tr}^f)^i$ is calculated by Eq. (49) where F_1^e is null and F_2^p and F_3^s are substituted by $(F^p)^{i-1}$ and $(F^s)^{i-1}$ respectively. Besides, $(L_{tr}^s)^i$ is determined by Eq. (33) where F_1^e is null and F_2^p is also replaced by $(F^p)^{i-1}$. Finally, $(L_{tr}^p)^i$ is given by

$$(L_{tr}^p)^i = L_f - (L_{tr}^s)^i - (L_{tr}^f)^i \tag{73}$$

Since free end undergoes plastic phase, $(\delta_F)^i$ is derived by Eq. (58) at $x^p = (L_{tr}^p)^i$. Then, $(F^p)^i$, $(F^s)^i$ and $(F^f)^i$ are obtained by Eqs. (59) at $x^p = (L_{tr}^p)^i$, (63) at $x^s = (L_{tr}^s)^i$ and (67) at $x^f = (L_{tr}^f)^i$ respectively. The total pullout force becomes

$$F^i = (F^p)^i + (F^s)^i + (F^f)^i \tag{74}$$

Elastic-Plastic-Softening-Frictional (Fig. 6)

When $\delta_L > \delta_3$ and $L_{tr}(\delta_L) < L_f$, L_f undergoes simultaneously the four proposed bond phases. By imposing a small increment for δ_L , the same strategy can be also applied in this case to determine $(L_{tr}^p)^i$, $(L_{tr}^s)^i$ and $(L_{tr}^f)^i$ by initially taking F_1^e , F_2^p and F_3^s equal to $(F^e)^{i-1}$, $(F^p)^{i-1}$ and $(F^s)^{i-1}$ respectively. Then, $(L_{tr}^e)^i$ is given by

$$(L_{tr}^e)^i = L_f - (L_{tr}^p)^i - (L_{tr}^s)^i - (L_{tr}^f)^i \tag{75}$$

and the following equation gives the total pullout force:

$$F^i = (F^e)^i + (F^p)^i + (F^s)^i + (F^f)^i \quad (76)$$

The flowchart of the proposed analytical-numerical algorithm is presented in Fig. 7. In all above cases, once $(L_{tr})^i$ is obtained for the all active bond phase (e.g. *Elastic*, *Plastic* and *Softening* are the active bond phase in case of Fig. 5a), the values of $(F^e)^{i-1}$, $(F^p)^{i-1}$, $(F^s)^{i-1}$ and $(F^f)^{i-1}$ are substituted respectively by the new calculated values of $(F^e)^i$, $(F^p)^i$, $(F^s)^i$ and $(F^f)^i$. Then, $(L_{tr})^i$ is recalculated until achieving a value of error less than a tolerance adopted for ΔL_{tr}. This calculation loop is also illustrated in the flowchart.

Outline of the experimental work

An experimental program comprising 36 pullout bending specimens was carried out by Mazaheripour et al. (2012a) in order to assess the bond behavior of GFRP bars embedded into SFRSCC. A test setup similar to that recommended by RILEM for case of steel bars was adopted. The test setup and the measuring devices are schematically shown in Figure 8. Two types of GFRP bars of ribbed (8 and 12 mm diameter) and smooth surface (only 12 mm diameter) that are commercially produced by European companies were utilized in the experimental tests. According to the data sheet provided by the suppliers, Young's modulus of the ribbed and smooth GFRP bars are, respectively, 56 and 49 GPa, while the ultimate tensile strengths are 1350 MPa and 1000 MPa. Additionally, a series of five notched beam bending tests (named as NB1 to 5) was carried out according to recommendations by CEB-FIP MC2010 in order to characterize the post-cracking behavior of the developed SFRSCC with 60 kg/m^3 of hooked ends steel fibers (length and diameter of 33 mm and 0.55 mm, respectively, and ultimate tensile strength of 1100 MPa). Figure 9 shows the configuration of notched beam bending test and the results in terms of Force-CMOD (crack mouth opening displacement) at notched cross section. Based on the force values, the derived residual flexural tensile stress parameters, f_R, were determined by

$$f_R = \frac{3PL}{2bh_{sp}^{\ 2}} \quad (77)$$

where P is the applied load; b and h_{sp} are the width and the height of the notched section, respectively. The values of f_R are also shown in the secondary vertical axis in Fig. 9. Moreover, the main mechanical properties of SFRSCC are included in Table 1.

In the bond tests, three bond lengths (L_f) of 5, 10 and 20 times of bar diameter (d_b) and two concrete cover thicknesses (C=15 and 30 mm) were the parameters whose influence on the bond behavior of GFRP/SFRSCC was investigated. With an exception of one pullout bending specimen regarding to GFRP bar of 8 mm diameter and 20d_b bond length, the remaining ones failed by debonding in which a residual pullout force was recorded for all of them. In case of ribbed GFRP

bars with concrete cover of 15 mm, a single crack appeared along the embedment length. However, splitting failure mode never occurred due to the contribution of fibers bridging this crack that had maintained the crack width at very small value. The reader is directed to the paper by Mazaheripour et al. (2012a) for more details about the experimental results.

Predictive Performance of the Bond Model

To assess the predictive performance of the proposed bond model, the obtained F-δ from the model is compared with the results registered in the previously described bond tests. The values of the parameters to define the τ-δ relationship in the model were calibrated using inverse analysis by minimizing the absolute value of error (e) which is defined as $\left|A_{F-\delta}^{the}-A_{F-\delta}^{\exp}\right|/A_{F-\delta}^{\exp}\times 100$, where $A_{F-\delta}^{\exp}$ is the area under the average F-δ of the experimental curves, and $A_{F-\delta}^{the}$ is the area of the F-δ obtained theoretically. Table 1 presents the results of the inverse analysis as well as the error (e), in percentage. In this table, the following experimental results are also reported: the maximum pullout force (F_{max}); its corresponding loaded end slip (δ_m) and the residual pullout force at the end of the tests (F_{res}) which was calculated for a pullout force corresponding to the relatively high value of slip (8 mm), when for all the specimens the debonding process was in the post-peak pullout force.

Loaded End Slip

The F-δ_L relationship registered experimentally and determined by the proposed bond model are compared in Fig. 10 and 11 for deformed and smooth GFRP bars, respectively. The results for the 8 mm bar diameter were not considered in the present study. This comparison evidences that the proposed method is capable of simulating with good accuracy the pullout force *versus* loaded end slip for the two types of GFRP bars. Moreover, the abrupt decay registered in the specimens reinforced with smooth GFRP bar's surface and $20d_b$ bond length (see Fig. 11) was properly captured by using the proposed bond model, whereas the previously developed model by Mazaheripour et. al. 2012b was practically unable to simulate this behavior.

Free End Slip

Figs. 12 and 13 compare the experimental and theoretical F-δ_F relationships. As shown, the proposed bond model also predicts with acceptable accuracy the slip at free loaded end. To understand better this accuracy, Fig. 14 represents the relationship between δ_L and δ_F obtained experimentally and theoretically for the specimens with L_f=$20d_b$. As shown, the $\delta_L-\delta_F$ curve obtained by the proposed bond model is in agreement with the experimental $\delta_L-\delta_F$ curve for both GFRP bars. This confirms the accurate prediction of the obtained $\delta(x)$ by the proposed bond model.

Observations

"Material" versus "structural" bond-slip property

Like in the present paper, the slip between bar and surrounding concrete is currently measured at the free and loaded ends by using displacement transducers. The slip is, therefore, the relative deformation between the concrete zones where the transducer is supported, and the section of the FRP bar where the other extremity of the sensor is connected. This means that the measure recorded by this sensor is always affected by the deformation of the concrete zone supporting the transducer, which is a quantity difficult to obtain with accuracy. By bonding strain gauges to the FRP bar along the embedment length is also another common alternative to measure indirectly the slip. Nevertheless, the slip variation along the embedment length can only be representative if a reasonable number of strain gauges are applied, which has, however, a detrimental effect on the bond conditions between the bar and the surrounding concrete. Furthermore, the strategy of converting strain values from these strain gauges into a slip concept between bar and surrounding materials is quite arguable, and only admissible if negligible deformation is assumed for the surrounding concrete. Considering all these aspects, a local bond-slip relationship only exists, and therefore considered as a material property, when the deformation and damage in the surrounding concrete is much smaller than the deformation in the FRP bar. This means that a local bond-slip relationship is a material property only if assessed from experimental data corresponding to FRP-concrete bond length short enough to avoid significant deformation and damage in the surrounding concrete. For the other cases the bond-slip relationship is a structural property, since the sensors are affected by the relevant deformation and damage formed in the surrounding concrete.

Due to these reasons, the bond length possibilities adopted in the present research are relatively small in order to maintain the deformability and the damages relatively small compared to the deformability of the FRP bars. Furthermore, due to the crack arrestment provided by the fibers bridging the micro-cracks, the damage due to crack formation in the surrounding concrete became limited. Therefore, for modeling the bond behavior between the GFRP bars and the SFRSCC considered in the present work, the bond-slip relationship derived from the tests with the lowest embedment length is recommended.

Theoretical bond strength and its corresponding slip

Taking the results from Table 2, which were obtained from inverse analysis, the influence of the bond length (L_f) on the value of the bond strength (τ_m) is represented in Fig. 15a. The τ_m shows tendency to decrease with the increase of L_f for a fixed concrete cover and type of GFRP bar. Additionally, the value of τ_m in case of 30 mm concrete cover was higher than that for 15 mm. The τ_m was also higher in deformed bar than in smooth bar's surface. However, in case of 15 mm concrete cover thickness, τ_m was similar for both types of GFRP bars, because the relatively low confinement provided

by this concrete cover thickness is not enough to mobilize the advantages of deformed bar surface characteristics. Hence, concrete cover higher than 15 mm (>1.25ϕ) is recommended for deformed GFRP bars in order to attain higher magnitude of bond strength (τ_m).

The influence of increasing L_f on the slip at the end of the plastic phase, δ_2, is also shown in Fig. 15b. By increasing L_f, δ_2 increased for both types of GFRP bar. This means that δ_2 is another parameter of the bond-slip constitutive law has increased with L_f for the same type of bar, concrete and concrete cover thickness.

Parametric study

Hereafter, a parametric study was carried out to evaluate the influence of the involved parameters on the maximum pullout force (F_{max}), namely: the bond shear strength (τ_m) and its corresponding slips (δ_1 and δ_2), bond length (L_f), longitudinal Young's modulus of the bar (E_{lb}), and the slip corresponds to the end of softening phase (δ_3) of bond-slip constitutive law. The study comprised six stages and for each stage, the influence of one parameter on F_{max} was appraised by considering three different values for L_f (5, 10 and 20d_b bond length) while a constant value was given to the rest of the parameters. Table 2 presents the range of given values to the parameter at each stage. The initial bond stress (τ_0) and bar diameter (d_b) considered as 1.0 MPa and 12 mm in all cases, respectively. Fig. 16(a) to (f) show the results of this parametric study. As shown, F_{max} is significantly influenced by L_f and τ_m (see Fig. 16a and b). The influence of δ_1 and δ_3 depends on the value given to δ_2. When the values of δ_2 and δ_1 (or δ_2 and δ_3) are close to each others, their influence on F_{max} is more visible (see Fig. 16(c) and (e)). On the whole, the impact of all these slip values and also the magnitude of E_{lb} on the F_{max} are not significant when the $L_f < 20d_b$.

Theoretical Development Length

The minimum transferred bond length required to reach the ultimate tensile stress (σ_{bu}) in the bar can be predicted by means of the proposed bond model. Based on the results of the pullout tests carried out by Mazaheripour et al. (2012a), the minimum development length of the GFRP bars would be higher than 20d_b since no tensile rupture reported for the GFRP bars in that study (with an exception of one specimen). On the other hand, according to the paramedic study presented in this paper, among the set of local bond-slip law's parameters, only L_f and τ_m showed significant influence on the maximum pullout force. Therefore, τ_m was defined as function of the bond length (L_f) in the proposed bond model. Accepting exponential fit for the τ_m-L_f, τ_m can be estimated with the following expression:

$$\tau_m(L_f) = b_1(L_f)^{b_2} \tag{78}$$

where b_1 and b_2 are the constant values fit the equation with the test results of different bond length (see Fig. 15a). By imposing Eq. (78) into the model instead of τ_m, the maximum pullout force is obtained for whatever value of L_f. The other parameters adopted in the bond model are summarized in Table 4.

Fig. 17 shows the achievable theoretical tensile stress (σ_b) for whatever value of (L_f/d_b) obtained from the bond model. These results were also compared with those values calculated from the formulation of several codes by means of the Eqs. (79), (80), (81) and (82) for given L_f/d_b and C/d_b:

$$\sigma_b = \frac{0.083\sqrt{f_c'}}{\alpha}\left(13.6\frac{L_f}{d_b}+\frac{C}{d_b}\frac{L_f}{d_b}+340\right) \quad (ACI\ 2006) \tag{79}$$

$$\sigma_b = 1.25\sqrt{f_c'}\left(0.318\left(\frac{L_f}{d_b}\right)+0.795\left(\frac{C}{d_b}\right)\left(\frac{L_f}{d_b}\right)+13.3\right) \quad (JSCE\ 1997) \tag{80}$$

$$\sigma_b = 54\left(\frac{f_c'}{25}\right)^{0.25}\left(\frac{25}{d_b}\right)^{0.20}\left(\frac{L_f}{d_b}\right)^{0.55}\left(\frac{C}{d_b}\right)^{0.33}\left(\frac{C_{\max}}{C}\right)^{0.1} \quad (fib\ 2010) \tag{81}$$

$$\sigma_b = 1.13\sqrt{f_c'}\cdot\frac{1}{k_1k_4}\left(\frac{L_f}{d_b}\right)\left(\frac{C}{d_b}\right) \quad (CSA\ 2000) \tag{82}$$

where α is modification factor which considered as 1.0 for test specimen's condition. C indicates the value of concrete cover thickness in mm. The compressive strength (f_c') of SFRSCC reported in Table 1. C_{max} is the maximum horizontal distance from the bar to concrete surface which equals to 69 mm for position of the GFRP bars in the cross-section of the experimental pullout (Mazaheripour et al. 2012a). k_1 and k_4 in Eq. (83) are bar location and bar surface factors respectively. The former equals to 1.0 for the installation of the GFRP bars in the test specimens and the later defines as a ration between the bond strength of FRP bars to that steel bars with the same diameter, but not greater than 1.0. Here, k_4 is also considered as 1.0. The Eq. (82) given by the *fib* is recommended for steel bars, however, this equation is also recommended for FRP bars as internal reinforcement for concrete (*fib* Bulletin 40, 2007). Note that the confinement effect provided by the transverse reinforcement was neglected in the above equations since no stirrup was applied to the test specimens.

In general the recommendations included in ACI, JSCE, *fib* and CSA do not predict the experiments, particularly for the case of the lower concrete cover (C/d_b=1.25). It can be concluded that these formulations might not be straightforwardly used for the types of GFRP bar and SFRSCC that studied in this paper.

Based on the obtained results, for deformed GFRP bar, the minimum bond lengths required to reach the σ_{bu} (1350 MPa reported by supplier) are around 38.5d_b and 30d_b for C/d_b equals to 1.25 and 2.5, respectively. These values for smooth GFRP bar (with σ_{bu} of around 1000 MPa specified by the supplier) are 26.5d_b and 20d_b. It is worth noticing that the maximum tensile stress obtained in the test for smooth bar were close to 1000 MPa in case of 20d_b bond length and 30 mm

concrete cover; however, no rupture was reported in the bar. That means σ_{bu} would be greater than the value reported by the manufacturer.

Conclusion

A theoretical bond model was developed to calibrate the parameters which define a multi-linear bond shear stress–slip relationship (τ-δ) able to estimate the bond behavior between SFRSCC and GFRP. The model involved data from the experimental tests, and using an analytical-numerical algorithm to solve the governing equation on bond phenomenon of the longitudinal bars. The proposed algorithm showed good accuracy comparing with the experimental result of bending pullout tests obtaining the distribution of the bond shear stress and slip over the bond transfer length.

Due to the complexity of taking concrete deformation in the second-order differential equations, the relative slip (δ) was assumed to be equal to bar's elongation resulting that the local τ-δ is dependent on the bond length. When the bond length is increased, the pullout force and consequently the force transferred to the surrounding concrete increases and lead to increase the amount of concrete damages over the interface which is normally formed as some inclined cracks over the embedded bar to concrete. A "material" versus "structural" bond-slip property was introduced. A local bond-slip law is a material property only when it is derived from pullout tests where the deformation and damage of the concrete surrounding the embedment FRP bar is marginal compared to the deformation of the FRP bar. This law can be used as the slip component of the constitutive law of an interface finite element, and a robust and reliable model should be adopted for modeling the behavior of the surrounding concrete up to its collapse. In the remaining cases the bond-slip relationship is a structural property.

The bond strength, which was theoretically obtained from the proposed model, was utilized to determine the development length of the GFRP bars at the ultimate limit state failed by tensile rupture in the bar. The values obtained by the model for the types of GFRP bars and concrete considered in this study showed a large discrepancy with the values recommended by the guideline of ACI committee 440 (American Concrete Institute ACI 2006), Japan Society of Civil Engineers (JSCE, 1997), CEB-FIB Model Code 2010 and Canadian Standards Association (CSA, 2000). That means, the recommendations by these guidelines may not be straightforwardly used for the reinforcing system adopted in this study.

Acknowledgment

This work is supported by FEDER funds through the Operational Programme for Competitiveness Factors – COMPETE and National Funds through FCT – Portuguese Foundation for Science and Technology under the project PTDC/ECM/105700/2008 – "DURCOST - Innovation in reinforcing systems for sustainable pre-fabricated structures of higher durability and enhanced structural performance".

References

American Concrete Institute (ACI). (2006). “Guide for the design and construction of structural concrete reinforced with FRP bars.” *ACI* 440.1R-06, Detroit.

Baena, M., Torres L., Turon, A., Barris C. (2009). “Experimental study of bond behavior between concrete and FRP bars using a pull-out test.” Composite Part: B, 40(8), 784-797.

Barris, C., Torres, L., Turon, A., Baena, M., Catalan, A. (2009). “An experimental study of the flexural behaviour of GFRP RC beams and comparison with prediction models” Composite Structures 91(3), 286–295.

Bianco, V., Barros, J. A. O., Monti, G. (2009). “Bond Model of NSM-FRP Strips in the Context of the Strengthening of RC Beams.” Journal of Structural Engineering, 135(6), 619-631.

CEB-FIB (2010), “CEB-FIB Model Code 2010 – Final draft”, Thomas Thelford, Lausanne, Switzerland.

CEB-FIB (2007). “FRP reinforcement in RC structures” Bulletin No. 40, *fib* Task Group 9.3, Lausanne, Switzerland.

Choi, D. U., Chun, S. C., Ha, S. S., (2012), “Bond strength of glass fibre-reinforced polymer bars in unconfined concrete.” Engineering Structures 34, 303–313.

Cosenza, E., Manfredi, G., and Realfonzo, R. (1997) ‘‘Behavior and modeling of bond of FRP rebars to concrete.’’ Journal of Composites for Construction, 1(2), 40–51.

CSA. (2000). “Canadian Highway Bridge Design Code” CSA-S6-06, Canadian Standards Association, Toronto, Canada.

Eligehausen, R., Popov, E. P., and Bertero, V. V. (1983). “Local bond stress-slip relationships of deformed bars under generalized excitations.” Rep. No. 83/23, Environmental Engineering Research Council, University of California, Berkeley, Calif.

Focacci, F., Nanni, A., Bakis, C. E. (2000). “Local bond-slip relationship for FRP reinforcement in concrete." Journal of Composites for Construction, 4(1), 24-31.

Gravina, R. J., Smith, S. T. (2008) “Flexural behaviour of indeterminate concrete beams reinforced with FRP bars” Engineering Structures 30(9), 2370–2380.

Hao Q., Wang Y., He Z., Ou J. (2009). “Bond strength of glass fiber reinforced polymer ribbed rebars in normal strength concrete.” Construction and Building materials, 23(2), 865-871.

Harajli, M., Abouniaj, M. (2010). “Bond Performance of GFRP Bars in Tension: Experimental Evaluation and Assessment of ACI 440 Guidelines.” Journal of Composites for Construction,14(6), 659-668.

He, Z., Tian, G. (2011). “Reliability-based bond design for GFRP-reinforced concrete.” Materials and Structures 44, 1477–1489.

JSCE. (1997). “Recommendation for Design and Construction of Concrete Structures using Continuous Fiber Reinforcing Materials” Concrete Engineering Series 23, Japan Society of Civil Engineers, Tokyo, Japan.

Li, F., Zhao, Q. L., Chen, H. S., Wang, J. Q., Duan, J. H. (2010). “Prediction of tensile capacity based on cohesive zone model of bond anchorage for fiber-reinforced polymer tendon.” Composite Structures, 92(10), 2400–2405.

Malvar, L. J. (1995). “Tensile and bond properties of GFRP reinforcing bars.” ACI Journal of Materials, 92(3), 276–2985.

Masmoudi, R., Masmoudi, A. Quezdou, M. B., Daoud, A. (2011). “Long-term bond performance of GFRP bars in concrete under temperature ranging from 20 ^{o}C to 80 ^{o}C.” Construction and Building Materials, 25(2), 486–493.

Mazaheripour, H., Barros, J., Sena-Cruz, J., Pepe, M., Martinelli, E. (2012a). “Experimental study on bond performance of GFRP bars in self-compacting steel fiber reinforced concrete.” Composite Structures, 25, 202-212.

Mazaheripour, H., Barros, J., Pepe, M., Giliberti, A., Martinelli, E. (2012b). “Experimental and theoretical study on bond behavior of GFRP bars in steel fiber reinforced self compacting concrete.” 4th International symposium on Bond in Concrete, Brescia, Italy.

Pecce, M., Manfredi, G., Realfonzo R., Cosenza E. (2001). “Experimental and analytical evaluation of bond properties of GFRP bars.” Journal of Materials in Civil Engineering, 13(4), 282–290.

RILEM. Bond test for reinforcement steel 1. Beam test. 1982; TC9-RC.

RILEM TC 162-TDF (2002), “Test and design methods for steel fiber reinforced concrete.” Materials and structures, 35, 579-582.

Russo, G., Zingone, G., Romano, F. (1990). “Analytical solution for bond-slip of reinforcing bars in R.C. joints.” Journal of Structural Engineering, 116(2), 336–355.

Sena-Cruz, J., Barros, J. (2004). “Strengthening of concrete structure with near-surface mounted CFRP laminate strips.” Computers and Structures, 82(17-19), 1513–1521.

Tang, W. C., Lo, T. Y., Balendran, R. V. (2008). “Bond performance of polystyrene aggregate concrete (PAC) reinforced with glass-fibre-reinforced polymer (GFRP) bars.” Building and Environment, 43(1), 98–107.

Tastani, S. P., Pantazopolou, S. J., (2006). “Bond of GFRP Bars in Concrete: Experimental Study and Analytical Interpretation.” Journal of Composites for Construction, 10(5), 381-391.

Zhang, B., Benmokrane, B., Chennouf, A. (2000). “Prediction of tensile capacity of bond anchorages for FRP tendons.” Journal of Composites for Construction, 4(2), 39-47.

NOTATION

A_b = area of the GFRP bar cross-section

A_s = constant in the expression of the softening phase transfer length

B_s = constant in the expression of the softening phase transfer length

C = SFRSCC cover thickness from the bottom surface

$C_{\max}$ = maximum concrete cover thickness from the concrete surface

C_s = constant in the expression of the softening friction transfer length

C_1^e = first integration constant for the elastic phase

C_2^e = second integration constant for the elastic phase

C_3^e = constant value for the elastic phase

C_1^f = constant value for the friction phase

C_2^f = first integration constant for the friction phase

C_3^f = second integration constant for the friction phase

C_1^p = constant value for the plastic phase

C_2^p = first integration constant for the plastic phase

C_3^p = second integration constant for the plastic phase

C_1^s = first integration constant for the softening phase

C_2^s = second integration constant for the softening phase

C_3^s = constant value for the softening phase

E_{lb} = young's modulus of GFRP bar

F = value of pullout force transferred by bond length

F_1^e = maximum value of force transferred in the elastic phase in case of infinite bond length

F^e = value of force transferred in the elastic phase in case of infinite bond length

F^f = value of force transferred in the friction phase in case of infinite bond length

$F_{\max}$ = value of the maximum experimental pullout force transferred by L_f

F_2^p = maximum value of force transferred in the plastic phase in case of infinite bond length

F^{p} = value of force transferred in the plastic phase in case of infinite bond length

F_3^s = maximum value of force transferred in the softening phase in case of infinite bond length

F^{s} = value of force transferred in the softening phase in case of infinite bond length

F_{res} = value of the residual pullout force obtained experimentally

J_1 = constant in the governing differential equation with unknown $\delta(x)$

L = span of the notched beams

L_f = available finite bond length

L_{tr1} = maximum invariant value of transfer length that can undergo elastic phase

L_{tr2} = maximum invariant value of transfer length that can undergo plastic phase

L_{tr3} = maximum invariant value of transfer length that can undergo softening phase

$L_{tr}(\delta_L)$ = transferred bond length corresponding to whatever value of the imposed slip

L_{tr}^{e} = transferred bond length undergoing elastic phase

L_{tr}^{f} = transferred bond length undergoing friction phase

L_{tr}^{s} = transferred bond length undergoing softening phase

L_{tr}^{p} = transferred bond length undergoing plastic phase

P = the vertical applied load in the notched beam tests

b = width of the notched beams

b_1 = first constant value of fitting equation expressed τ_m-L_f relationship

b_2 = second constant value of fitting equation expressed τ_m-L_f relationship

d_b = diameter of GFRP bars

e = error between experimental and theoretical pullout force-slip curves

h_{sp} = height of the notched section of the beams

i = number of the calculation step

f_c' = the compressive strength of SFRSCC

f_R = the residual flexural tensile stress of SFRSCC

k_1 = bar location factor in equation in Eq. (67)

k_4 = bar surface factor in equation in Eq. (67)

x^e = local references system in elastic phase

x^f = local references system in frictional phase

x^s = local references system in softening phase

x^p = local references system in plastic phase

$\Delta\delta$ = slip increment in the calculation

α = modification factor for recommended equation from ACI

β = constant entering the governing differential equation for the softening phase

ϕ = angle necessary to determine the softening-subject amount of transfer length

δ = relative displacement between bar and surrounding concrete along the bond length

δ_1 = first value of slip corresponding to peak of local bond stress-slip relationship

δ_2 = second value of slip corresponding to peak of local bond stress-slip relationship

δ_3 = slip corresponding to the start of frictional phase in bond stress-slip relationship

δ_F = free end slip

δ_m = slip experimentally recorded at the loaded end corresponding to F_{max}

δ_L = imposed slip at the loaded extremity of the bar

δ^e = slip along the amount of transfer length in elastic phase

δ^f = slip along the amount of transfer length in frictional phase

δ^s = slip along the amount of transfer length in softening phase

δ^p = slip along the amount of transfer length in plastic phase

λ = constant entering the governing differential equation for elastic phase

$\tau(\delta)$ = bond shear stress-slip relationship

τ = bond shear stress

τ_0 = chemical initial bond stress of GFRP-SFRSCC

τ_m = peak stress of the local bond stress-slip relationship

τ_R = residual bond shear stress

σ_b = the achievable theoretical tensile stress of GFRP bars

σ_{bu} = the ultimate tensile stress of GFRP bars

Tables

Table 1. Mechanical properties of SFRSCC

	Compressive strength (MPa)	Flexural tensile strength[1] (MPa)	Young's modulus (MPa)
SFRSCC	63.68 [2]	6.48	30360 [3]
(CoV)	(5.51%)	(17.49%)	(15.48%)

[1] Equal to *Limit of Proportionality* according to CEB-FIB MC2010 (CMOD=0.05 mm)
[2] Mean value of 15 specimens
[3] Mean value of 3 specimens

Table 2. Relevant experimental results and values of the parameters of the bond model obtained from the inverse analysis

		Experimental results			The results from the bond model							
L_f		F_{max} (kN)	δ_m (mm)	F_{res} (kN)	τ_0 (MPa)	τ_m (MPa)	τ_R (MPa)	δ_1 (mm)	δ_2 (mm)	δ_3 (mm)	τ_R/τ_m (%)	e (%)
Deformed GFRP bar, 12 mm diameter												
$5d_b$	C15:	44.76	0.33	17.64	1.0	18.1	7.6	0.09	0.15	2.30	41.5	0.87
	C30:	57.49	0.29	19.75	1.0	23.2	14.8	0.07	0.19	1.50	64.4	0.57
$10d_b$	C15:	70.62	0.84	31.59	1.0	14.3	6.8	0.09	0.50	5.0	46.6	0.63
	C30:	89.54	1.34	40.99	1.0	18.3	8.7	0.15	0.70	5.2	47.4	0.01
$20d_b$	C15:	121.81	2.56	50.22	1.0	12.5	5.1	0.12	1.80	7.0	39.0	0.48
	C30:	146.23	3.00	61.63	1.0	14.9	5.9	0.11	1.20	8.6	33.9	2.63
Smooth GFRP bar, 12 mm diameter												
$5d_b$	C15:	42.06	0.47	18.63	1.0	18.0	8.3	0.10	0.16	1.1	47.2	0.80
	C30:	50.815	0.44	38.73	1.0	21.9	13.1	0.09	0.15	1.1	60.5	0.97
$10d_b$	C15:	62.92	0.81	28.08	1.0	14.0	6.0	0.10	0.35	1.9	42.7	1.09
	C30:	76.64	1.50	42.06	1.0	16.5	9.0	0.10	0.55	2.0	50.5	2.60
$20d_b$	C15:	98.74	2.04	54.47	1.0	12.2	5.8	0.10	0.5	2.0	44.7	1.23
	C30:	106.24	2.36	70.06	1.0	13.2	7.6	0.10	0.7	2.0	50.7	1.20

Table 3. Values of parameters adopted for parametric study *

Stage	d_b mm	τ_0 MPa	τ_m MPa	τ_R MPa	δ_1 mm	δ_2 mm	δ_3 mm	E_{lb} GPa	L_f mm
Study 1	12	1	**5-25**	$0.5\tau_m$	0.1	0.2	3	60	**5, 10, 20, 25, 30d_b**
Study 2	12	1	**14, 16, 18**	$0.5\tau_m$	0.1	0.2	3	60	**5d_b -30d_b**
Study 3	12	1	18	$0.5\tau_m$	**0.01-0.5**	**1, 2, 3δ_1**	3	60	**5, 10, 20d_b**
Study 4	12	1	18	$0.5\tau_m$	0.1	**0.1-2**	3	60	**5, 10, 20d_b**
Study 5	12	1	18	$0.5\tau_m$	0.1	**0.1, 0.3, 0.5δ_3 1-5**		60	**5, 10, 20d_b**
Study 6	12	1	18	$0.5\tau_m$	0.1	0.2	3	**30-65**	**5, 10, 20d_b**

Table 4. The parameters adopted in the model to obtain the maximum tensile stress for whatever value of L_f

GFRP		d_b (mm)	E_{lb} (GPa)	δ_1	δ_2 (mm)	δ_3	τ_0 (MPa)	τ_m *		τ_R (MPa)
								b_1	b_2	
Deformed bar	C15:	13.08	56.0	0.10	0.50	3.0	1.0	55.41 (R^2=0.96)**	-0.276	$0.5\tau_m$
	C30:	13.08	56.0	0.10	0.50	3.0	1.0	86.70 (R^2=0.99)	-0.323	$0.5\tau_m$
Smooth bar	C15:	12.36	49.0	0.10	0.50	2.0	1.0	58.61 (R^2=0.95)	-0.291	$0.5\tau_m$
	C30:	12.36	49.0	0.10	0.50	2.0	1.0	100.09 (R^2=0.99)	-0.373	$0.5\tau_m$

* Obtained from Eq. (63); ** Coefficient of determination;

Figures

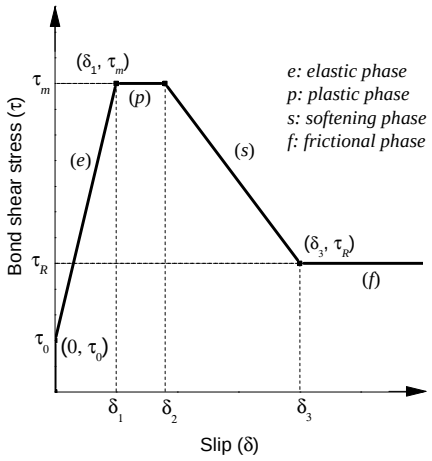

Fig. 1. The local bond shear stress-slip relationship

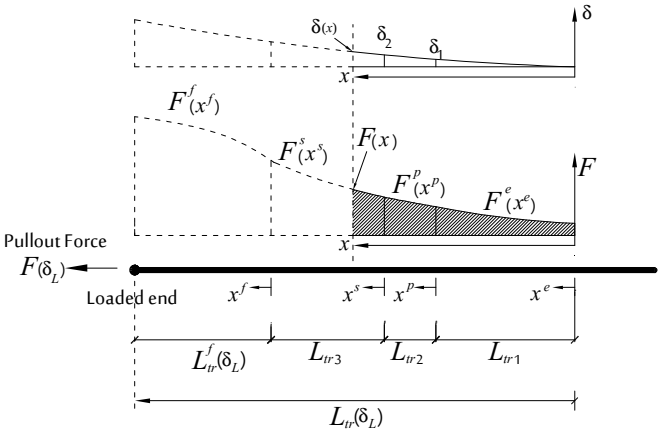

Fig. 2. Debonding process in case of infinite bond length: pullout force, $F(x)$, slip distribution, $\delta(x)$, the required transfer bond length, $L_{tr}(\delta_L)$, and definition of local reference systems

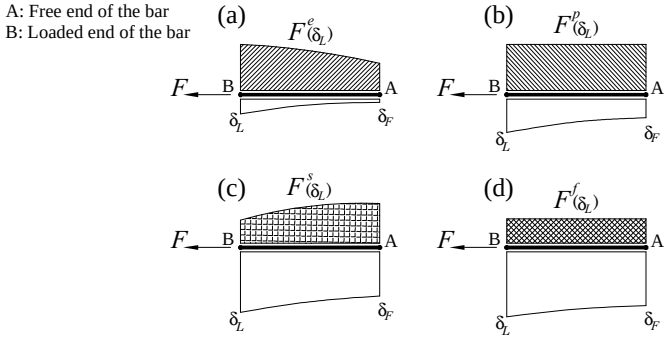

Fig. 3. The configurations for $\delta(x)$ and $F(x)$ over L_f when one bond phase is acting: (a) Fully Elastic, (b) Fully Plastic, (c) Fully Softening, (d) Fully Frictional

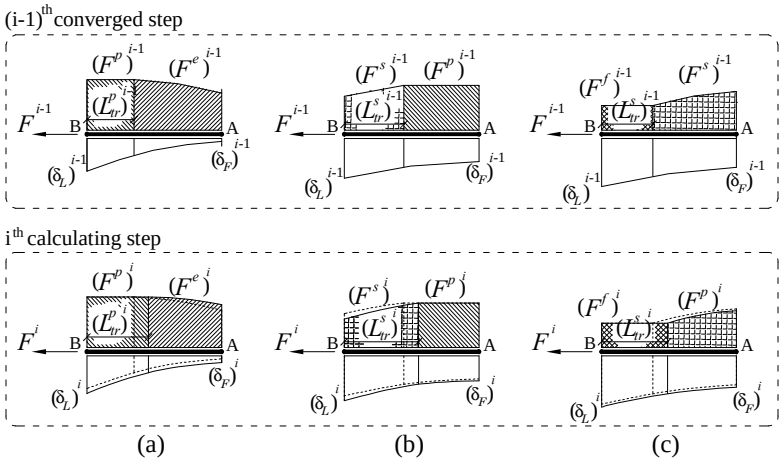

Fig. 4. The configurations for $\delta(x)$ and $F(x)$ over L_f when two bond phases are acting (a) Elastic-Plastic, (b) Plastic-Softening, (c) Softening-Frictional

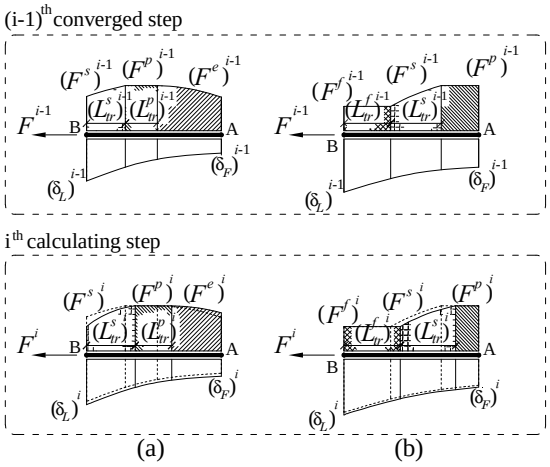

Fig. 5. The configurations for $\delta(x)$ and $F(x)$ over L_f when three bond phases are acting: (a) Elastic-Plastic-Softening (b) Plastic-Softening-Frictional

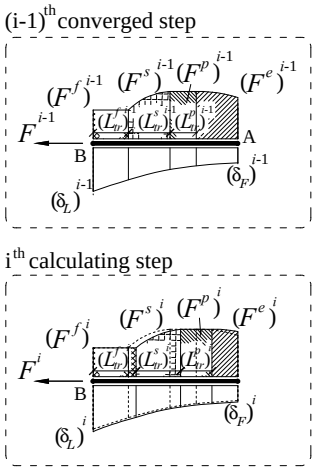

Fig. 6. The configurations for $\delta(x)$ and $F(x)$ over L_f when four bond phases are acting: Elastic-Plastic-Softening-Frictional

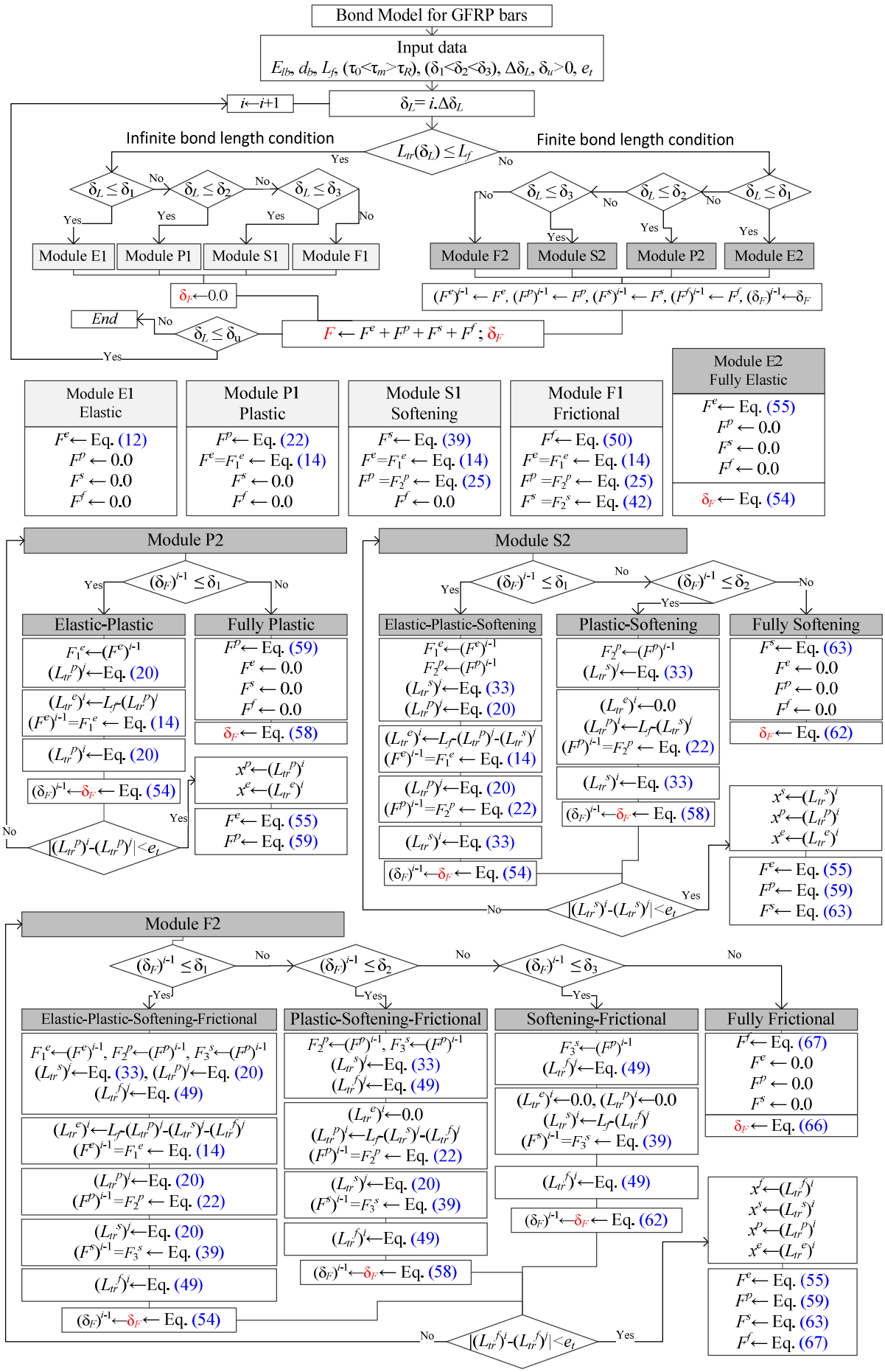

Fig. 7. Flowchart of the proposed bond model

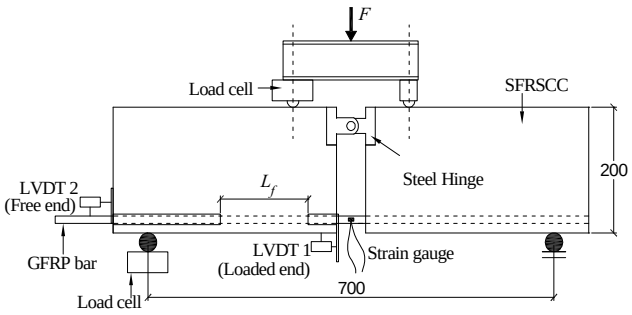

Fig. 8. The pullout bending test setup (Mazaheripour et al., 2012a)

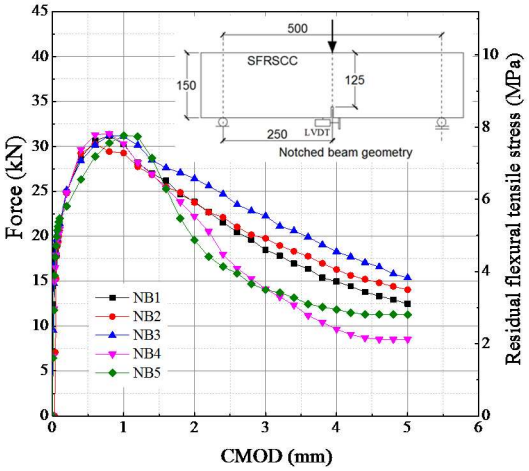

Fig. 9. The results of the notched beam bending tests carried out to characterize the SFRSCC

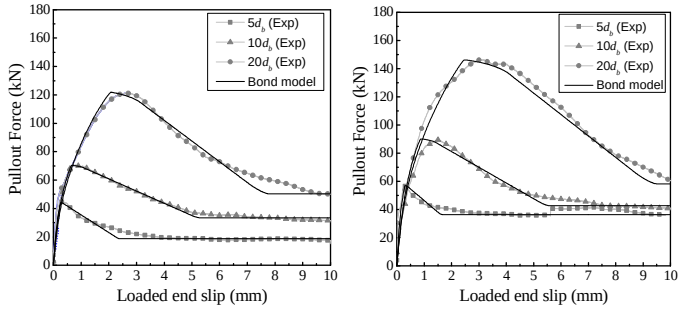

Fig. 10. The comparison between theoretical and experimental pullout force *versus* loaded end slip for deformed GFRP bar: (a) 15 mm and (b) 30 mm concrete cover

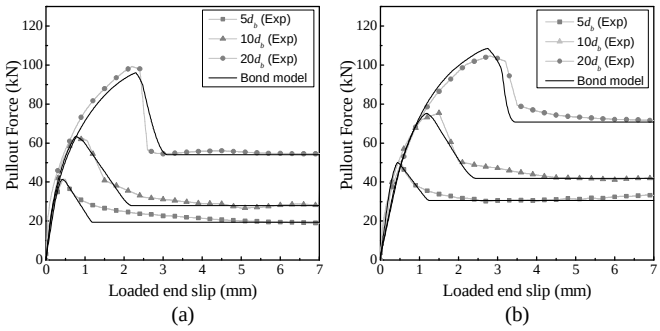

Fig. 11. The comparison between theoretical and experimental pullout force *versus* loaded end slip for smooth GFRP bar: (a) 15 mm and (b) 30 mm concrete cover

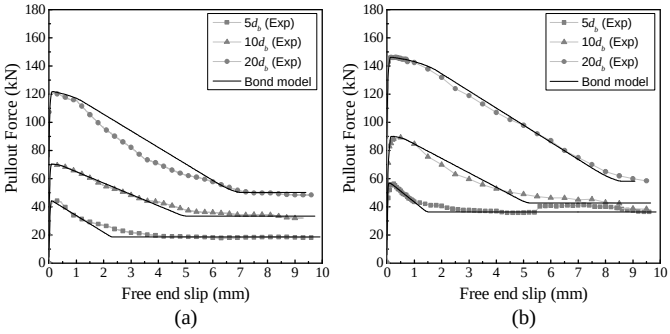

Fig. 12. The comparison between theoretical and experimental pullout force *versus* free end slip for deformed GFRP bar: (a) 15 mm and (b) 30 mm concrete cover

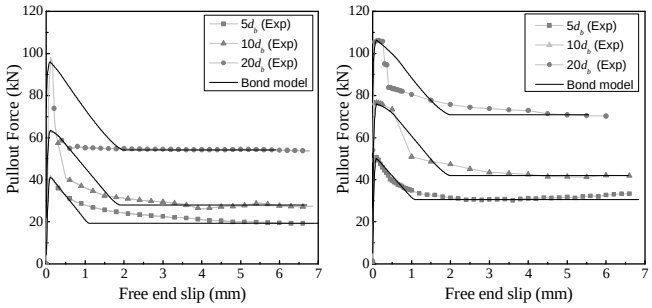

Fig. 13. The comparison between theoretical and experimental pullout force *versus* free end slip for smooth GFRP bar: (a) 15 mm and (b) 30 mm concrete cover

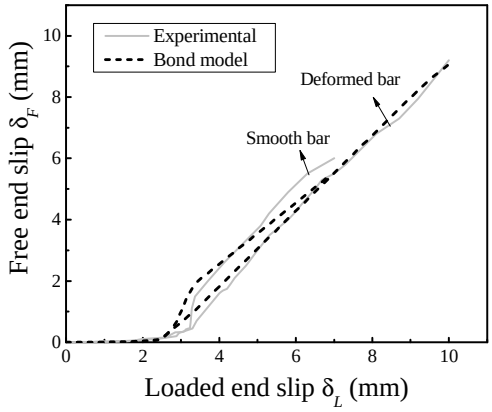

Fig. 14. The relationship between loaded and free end slip (δ_L-δ_F) for specimen with L_f=20d_b

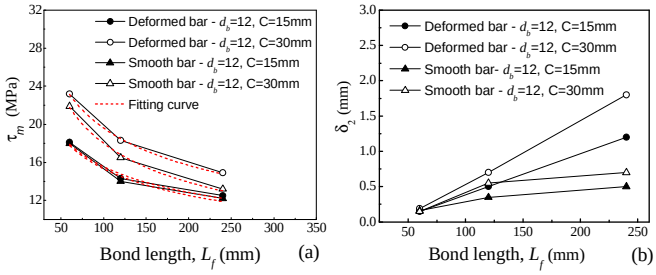

Fig. 15. (a) the analytical bond strength (τ_m) and (b) corresponding slip at the end of the plastic phase (δ_2) *versus* bond length (L_f)

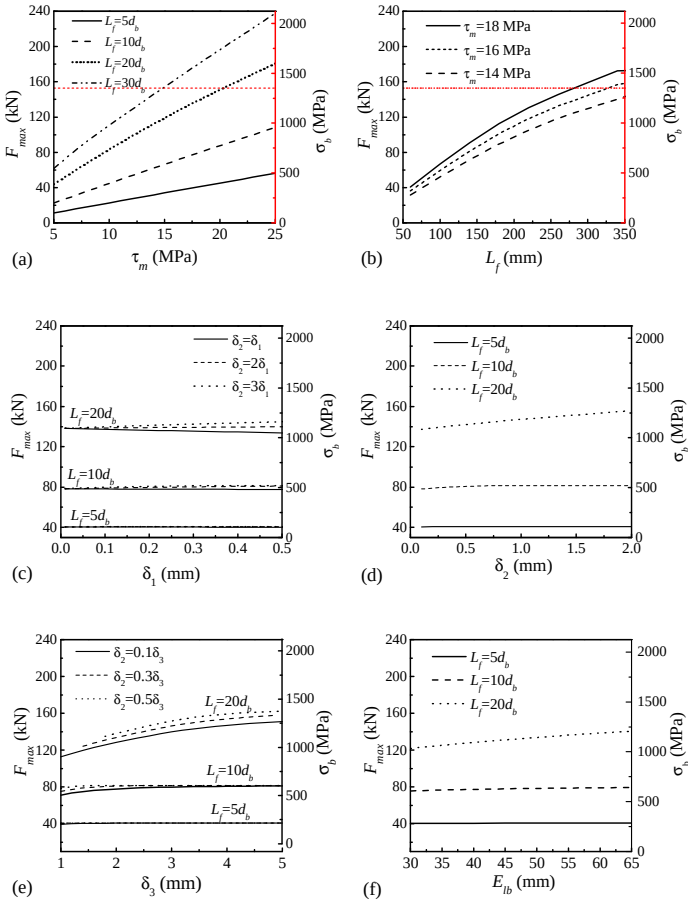

Fig. 16. Appraisal of influence of (a) the maximum bond stress; (b) bond length; (c) slip at the end of elastic phase (δ_1); (d) slip at the end of plastic phase (δ_3); (e) slip at the end of softening phase; (f) GFRP' Young's modulus on maximum force transferred by bond length

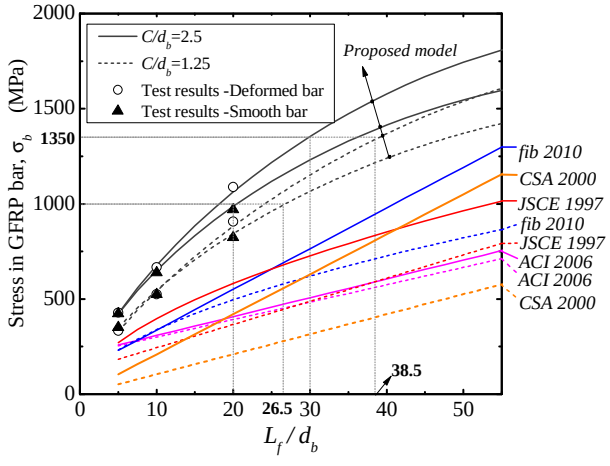

Fig. 17. The tensile stress of GFRP bars versus L_f/d_b